University of California Riverside

ME170B Experimental Techniques: Lab 6

Wind Tunnel

Group A5

Elijah Perez | Soham Saha | Alex Pham

Fall 2024 - Mon-Wed 8AM Session

October 25th, 2024

Abstract

The purpose of this experiment was to identify the most aerodynamic object among four candidates, determine the influence of wind speed on normal and drag forces, and investigate the effects of angle of attack and pitch on the system, and plot the relationships between wind speed, normal force and drag, angle of attack, and pitch. The four objects selected were a wooden ellipsoid, red sphere, flat disk, and inverted hemisphere. It is hypothesized that the wooden ellipsoid will have the smallest drag coefficient of the four selected shapes, and that wind speed would increase drag forces and that angle of attack would also increase drag forces. The frontal area of each object was calculated by measuring diameters, and the selected objects were mounted one by one on a sting balance inside of a wind tunnel. The forces on the object were recorded and analyzed using AeroLab software. For each experiment wind speed and angle of attack were set while axial and normal force was measured directly through AeroLab software. The results were used to calculate the drag force, using the drag force equation in relation to axial and normal forces, along with comparing the calculated drag force to the theoretical drag force. The results of the experiment found the wooden ellipsoid to have the least drag coefficient, making it the most aerodynamic. On average, it had a drag coefficient of 0.0105 (75.5% error compared to theoretical value). Additionally it was observed that an increased angle of attack resulted in a higher drag coefficient for all four objects and higher lift coefficient. The findings of this experiment have numerous applications in any project where aerodynamics is involved.

Introduction

The study of aerodynamics plays a crucial role in many applications, namely aerospace and automotive engineering. Studying the effect of air on various shaped objects is fundamental to optimizing for aerodynamic efficiency, safety and reducing fuel consumption for both aerospace and automotive vehicles. The field of aerodynamics is centered around the concept of drag force, or the force exerted on an object in a submerged fluid. Minimizing the drag force is typically desired in most engineering applications.

The lab will analyze four objects of different geometries (wooden ellipsoid, red sphere, flat disk, and inverted hemisphere) to determine which is the most aerodynamic, or having the smallest drag coefficient. Additionally, the experiment seeks to assess whether wind speed impacts normal and drag forces, as well as the effects of angle of attack and pitch on the system's overall performance. Data will be used to construct plots showing the relationships between wind speed, normal force, drag, angle of attack, and pitch. Subsonic wind tunnels, like the one used in this experiment, are crucial tools in the aerospace and automotive industries, enabling engineers to optimize object geometries to reduce drag or increase lift, ultimately improving performance. This experiment will employ an AEROLAB Educational Wind Tunnel with AeroLab software to directly measure axial force, normal force, and air velocity experienced by the objects to calculate drag force.

It is hypothesized that the results of the experiment will suggest that the wooden ellipsoid will be the most aerodynamic. The wooden ellipsoid is chosen above the other objects based on its low frontal area, as well as its streamlined shape compared to the other objets. It is also predicted that increasing wind speed will result in higher drag and lift forces. Finally, it is predicted that increasing the angle of attack will also increase drag and lift forces.

Theory and Analysis

To determine which of the four objects is most aerodynamic, we will calculate the drag force using the recorded data from AeroLab and the following equation.

$$F_D = \frac{1}{2}\rho C_D A v^2 \qquad \textbf{Eq 1}$$

Equation 1 shows the drag force F_D in relation to frontal area *A*, velocity *v*, fluid density ρ, and drag coefficient C_D. We are interested in calculating the drag coefficient, by measuring all the other parameters in this equation. The drag coefficient is an object's dimensionless quantity used to quantify the resistance the object will experience. A lower drag coefficient means a more aerodynamic object.

and being the lift force acting upwards, perpendicular to the direction of airflow.

The theoretical drag force can be determined from the fluid's properties; density, ϱ, and speed, v; along with the object's contact surface area, A, and drag coefficient, CD.

$$F_L = \frac{1}{2}\rho C_L A v^2 \qquad \textbf{Eq 2}$$

Equation 2, is similar to equation one, and shows the lift force F_L in relation to frontal area *A*, velocity *v*, fluid density ρ, and drag coefficient C_L. Similar to the drag coefficient, we are interested in calculating the lift coefficient by measuring all the other parameters in this equation. The lift coefficient, similar to the drag coefficient, is also a dimensionless parameter that determines how much lift force an object will experience when moving past a fluid.

Experimental Methods

Safety Precautions

Keep a safe distance from the tunnel's exhaust area and remain cautious of any potential flying debris at all times. Do not open the wind tunnel door while the turbine is spinning. When operating the wind tunnel, ensure that wind speeds do not exceed 100 mph, the wind tunnel is not running at max velocity and that the sting balance's angle does not exceed ±30°.

Procedure

Before starting, launch the AeroLab software from the desktop; the system is pre-calibrated, so additional calibration is not required. Measure the temperature and humidity of the wind tunnel using a psychrometer and thermometer. Enter these values in the Aerolab software. Now measure the frontal area of all four objects (see appendix).

Handle the sting balance with care, ensuring it remains parallel to the wind tunnel. The pitch angle should be set to 0° using the digital protractor provided. Securely attach the object of interest to the sting balance as illustrated in Figure 7. Ensure that both the angle of attack and pitch are set to 0°.

To begin the experiment, turn on the wind tunnel fan and slowly rotate the speed control knob clockwise to set the wind speed to approximately 15 MPH. Allow the system to warm up for five minutes. Adjust the fan control knob to reach the desired wind speed and begin collecting data. Using the AeroLab interface (as shown in Figure 8), record the axial force, normal force, wind velocity, and pitch for each trial. Gradually increase the wind velocity to two or three additional values, documenting the same variables each time.

After completing the initial trials, adjust the pitch angle to a different value and repeat the process, ensuring you collect data for each speed and pitch variation. Pitch angle may be altered while the tunnel is active but the window panel must remain shut during wind tunnel operation. Once data collection for the first object is complete, repeat the entire procedure for the remaining three objects, following the same steps. Ensure that all safety measures are strictly observed throughout the process, including careful handling of the equipment and monitoring of wind speeds to avoid exceeding operational limits.

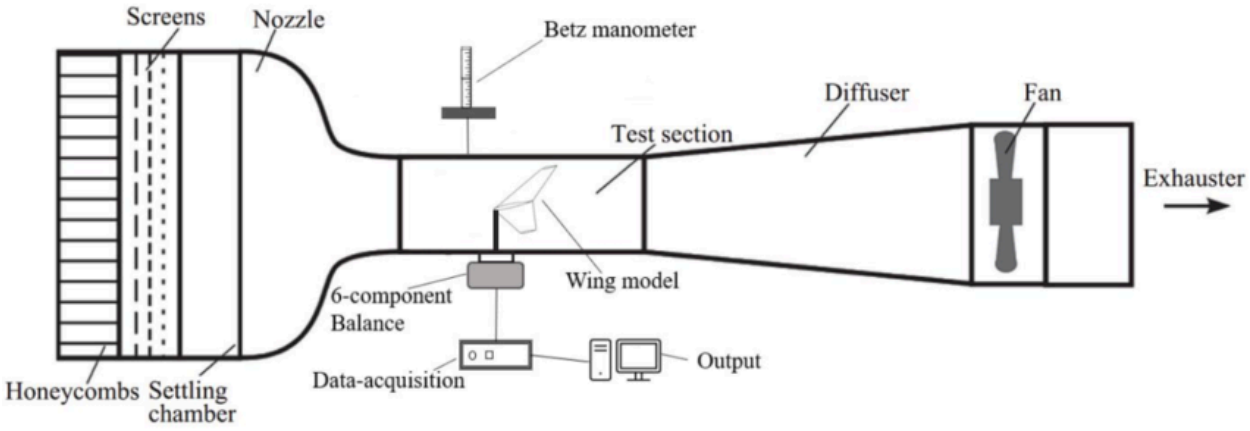

Figure 1: General schematic design of the subsonic wind tunnel

Data Analysis

Data from Aerolab can be exported into an Excel file. For our data collection, we took 10 snapshots with 10 samples each, including data for velocity, axial force, and normal force all measured by Aerolab. This was converted to values of Cd and Cl using a Matlab script and Equations 1 & 2 and then plotted to display relationships. Since each Excel file represented a unique experiment, experiments of the same shape were combined into plots to view the effect of wind speed and angle of attack on the drag and lift forces. This allows for a qualitative analysis of the effects of wind speed and angle of attack on the drag coefficient.

Results

Four distinct objects of varying shapes were tested under a range of wind speeds to determine their aerodynamic properties. The objects included a flat disk, an inverted hollow hemisphere, a large sphere, and a wooden ellipsoid. Figures 2-7 illustrate the results at three different wind speeds and pitch angles. At a wind speed of 50 mph with a 0° pitch angle, the drag forces for the flat disk, inverted hollow hemisphere, large sphere, and wooden ellipsoid were measured as 0.094 N, 0.1063 N, 0.0677 N, and 0.0095 N, respectively. These results confirm that the wooden ellipsoid was the most aerodynamic shape since it had the lowest drag force, as predicted.

From the data and plots, several trends were identified. A direct relationship between wind speed and both drag and normal forces was observed. As wind velocity increased, the drag force also increased for all shapes. For the normal force, the results varied depending on the pitch angle. At certain pitch angles, the normal force increased, while at others, it decreased. This variation and uncertainty can be explained by the measurement setup, where the direction of the normal force depends on the orientation of the object relative to the airflow. For instance, when

the tip of the object faced down, the normal force pointed downward; when the tip faced up, the normal force pointed upward. When accounting for this, the data consistently shows that an increase in air velocity leads to an increase in normal force. The fluctuations visible in the graphs below may be indicative of various aspects of flow in the wind tunnel which are beyond the scope of this experiment as well as a source of uncertainty. This may be related to laminar and turbulent flow around the object. Additionally, it is important to note that a logarithmic scale is used on all the plots to visually highlight the differences between low drag coefficients and high drag coefficients. This allows us to show 6 experiments for the same object in every plot. Without this, lower drag coefficients would all appear to be the same with minimal differences between experiments.

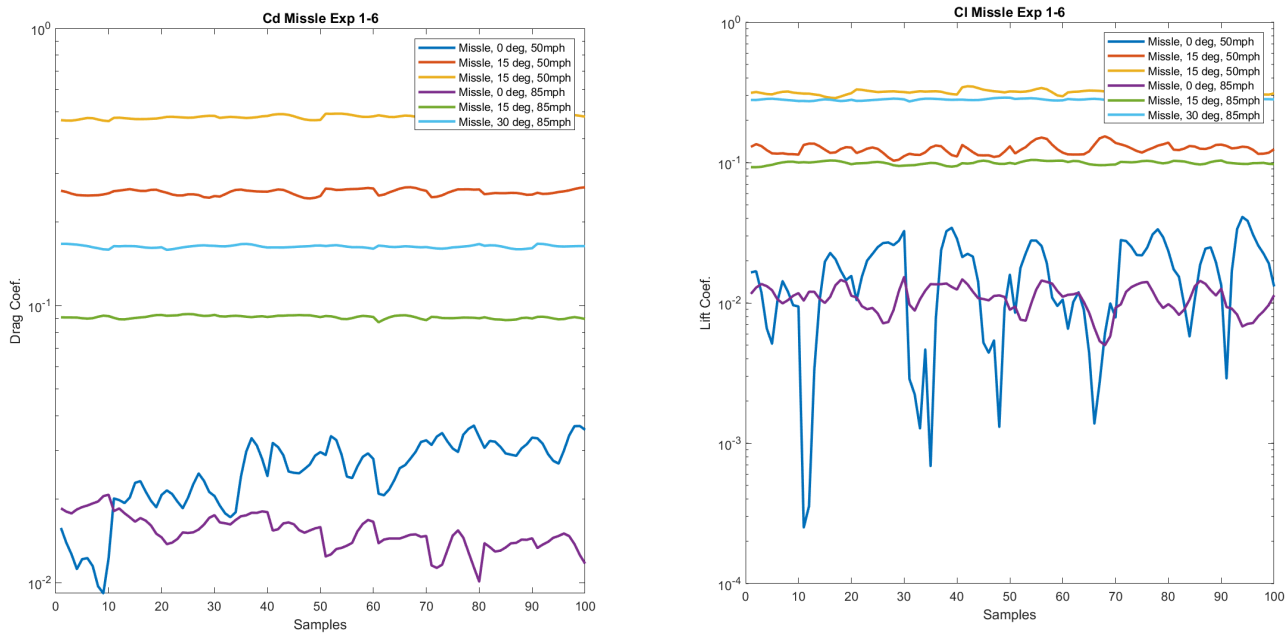

Figure 2: Drag (Cd) and Lift (Cl) coefficients for Wooden Ellipsoid (missile) shape for 6 experiments with varied wind speed and angle of attack . Note that yellow lines are intended to read *30deg, 50mph* in the legend.

The graphs in Figure 2 show how changes in wind speed and the angle of attack influence the aerodynamic efficiency of the object by affecting the drag coefficient. Higher wind velocities

and varying angles of attack cause noticeable fluctuations in Cd, reflecting the wooden ellisoids's resistance to airflow under different conditions

In observing Figure 2, we can see that the highest drag and lift coefficient for the wooden ellipsoid (missile) was found in the yellow lines, which corresponds to a *30º angle of attack*. This shows that increasing angle of attack increases both drag and lift forces, a phenomenon commonly observed in aircraft. As an aircraft approaches its desired altitude, it sets a large angle of attack to generate a stronger lift force so it may climb higher. This is one of many applications of the effect of angle of attack on lift coefficient. The major fluctuations in the lift coefficient graph for the dark blue line are a result of the logarithmic scaling which amplifies small differences. The sudden drops in lift coefficient may be a result of experimental uncertainties surfacing at very small lift coefficient values.

This can also be seen in Figure 3, where the light blue line (representing a 30º angle of attack with the sphere) also produced the greatest drag forces compared to other angles. Interestingly, for the sphere we do not see a huge variation in lift force with angle of attack. This may indicate that the sphere is a poor shape for generating lift.

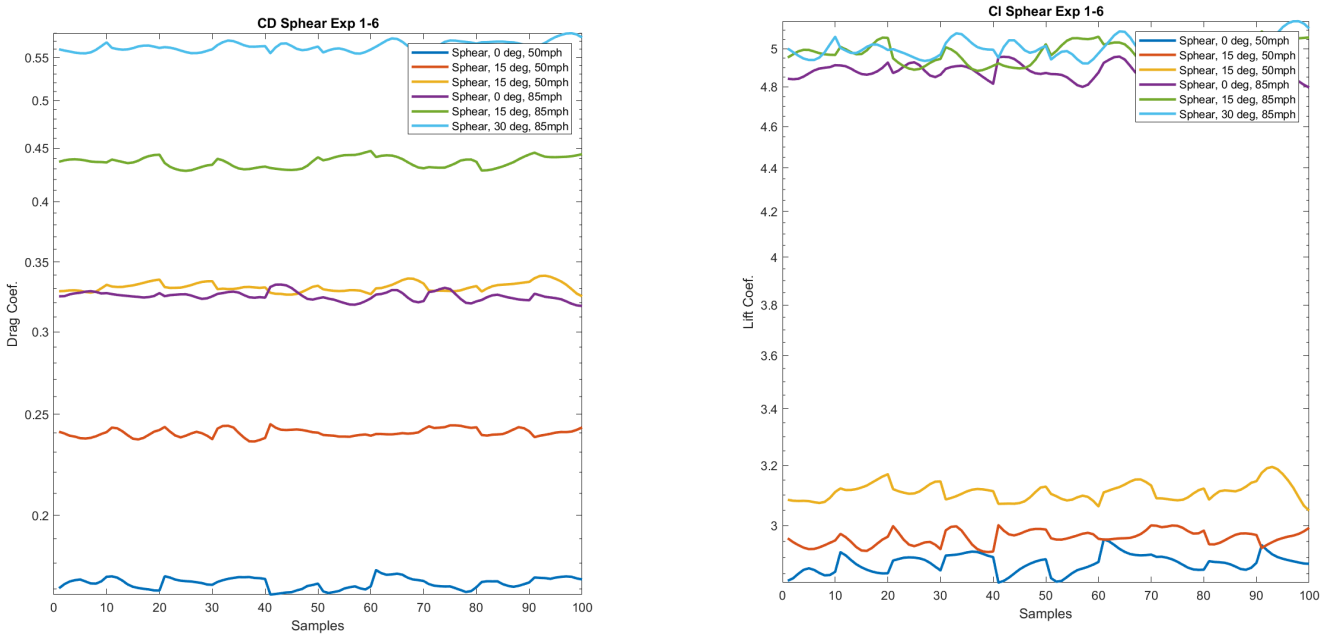

Figure 3: Drag (Cd) and Lift (Cl) coefficients for Red Sphere shape for 6 experiments with varied wind speed and angle of attack.

Figure 3 illustrates the impact of wind velocity and angle of attack on the raw calculation of the drag/lift coefficients (Cd) and (Cl). Here we can notice that the lift coefficient significantly increases with wind velocity.

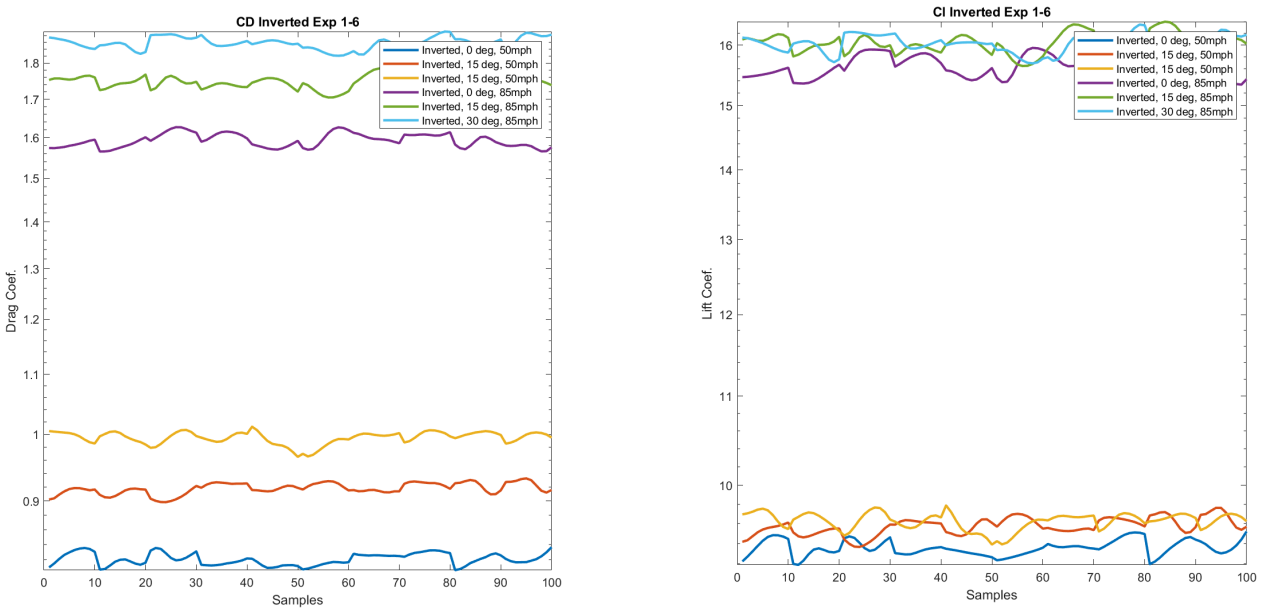

Figure 4: Drag (Cd) and Lift (Cl) coefficients for Inverted Hemisphere shape for 6 experiments with varied wind speed and angle of attack.

Figure 4 illustrates the impact of wind velocity and angle of attack on the raw calculation of the drag/lift coefficients (Cd) and (Cl). Here we can notice the large values in the lift coefficient and drag coefficient. The inverted hemisphere geometry is significantly less aero-dynamic as it has a high drag coefficient, but has the highest lift coefficient of all the shapes.

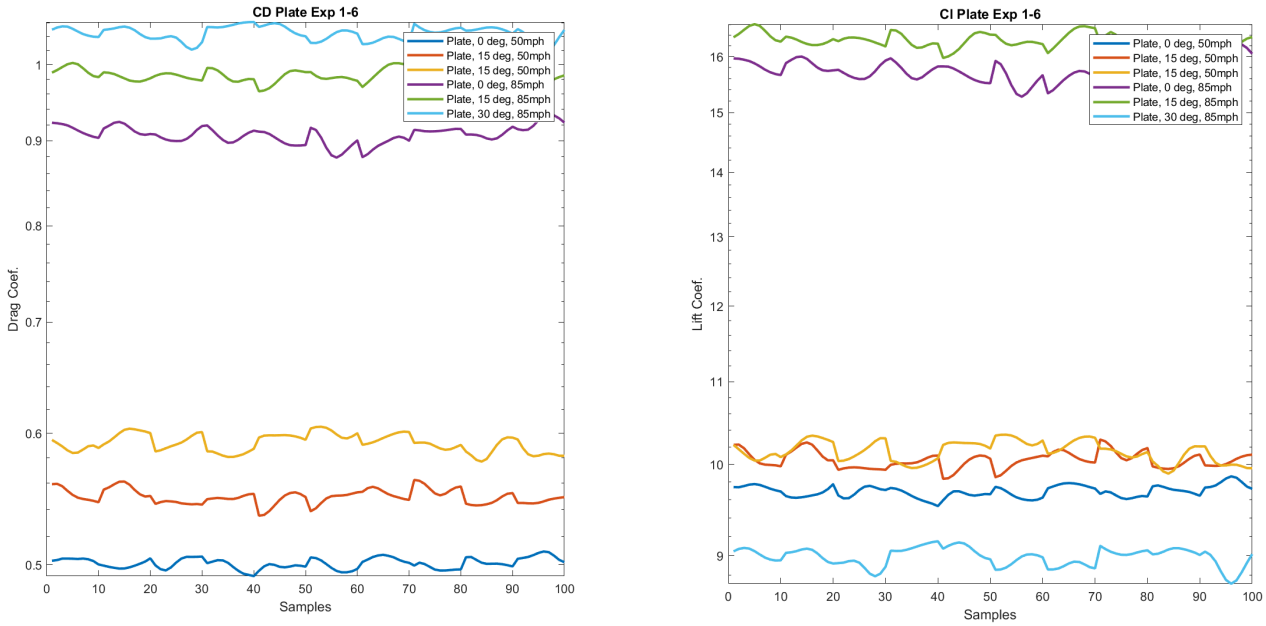

Figure 5: Drag (Cd) and Lift (Cl) coefficients for Inverted Hemisphere shape for 6 experiments with varied wind speed and angle of attack.

Figure 5 illustrates the impact of wind velocity and angle of attack on the raw calculation of the drag/lift coefficients (Cd) and (Cl). Here we notice the lift coefficient for the plate at 30 degrees and 85 Mph (light blue line in right graph) is lower than the rest of the data. We believe this could be due to system errors or a data collection error during the experiment.

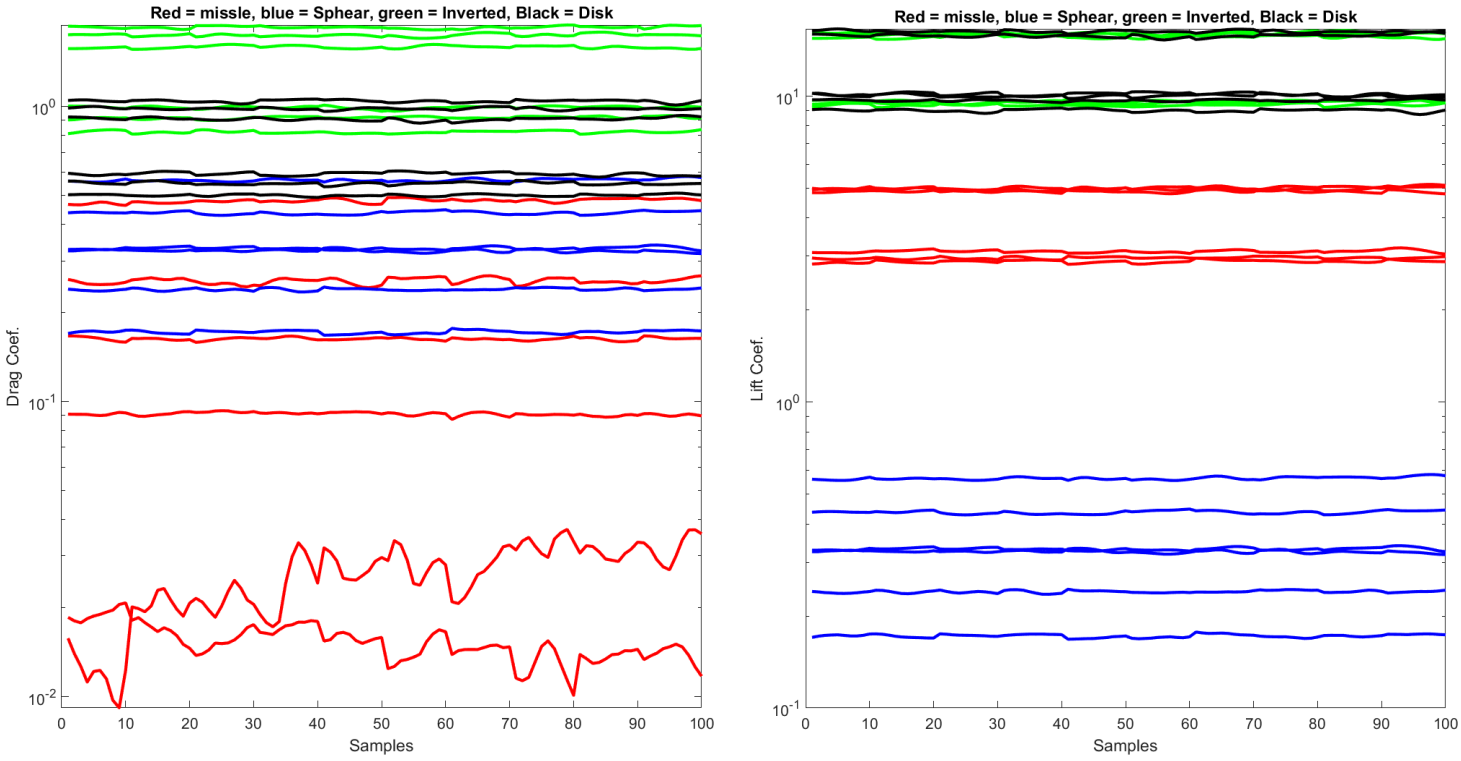

Figure 6: Overlaid graphs for drag and lift coefficient for all experiments of all 4 shapes. Shapes are color coded according to legend.

In Figure 6 we see similar graphs from the past figures, but now they are all overlaid on each other. The title of the graph describes the shape-to-color correlation. Here we can see that on average the inverted hemisphere has the largest drag and lift coefficients, thus projecting a larger reaction force. On the other hand, the wooden ellipsoid (missile) has the smallest drag coefficient giving it the smallest reaction force, making the missile the most aero-dynamic object. The object with the least amount of lifting force is the sphere.

In observing Figure 6, we can see how the different shapes compare to each other in regards to their drag and lift coefficients. Most notably we can see that the wooden ellipsoid had the least drag coefficient of all shapes. We can also see that the inverted hemisphere had the highest drag coefficient. These results are in line with our general intuition and match our predictions. Interestingly, we can also see that the sphere had the lowest lift coefficients, and the wooden ellipsoid had the second lowest. While none of the shapes used in the experiment are ideal for generating lift, we can see that the symmetrical shape of the sphere made it the worst candidate of these four.

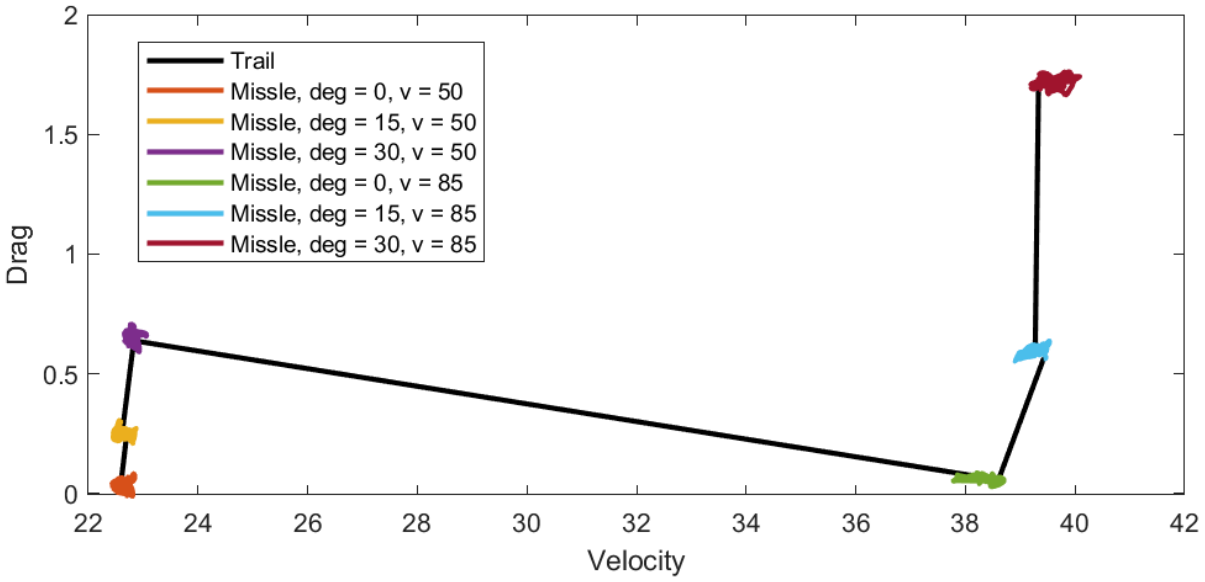

Figure 7: This graph presents the drag coefficient (Cd) versus velocity, based on experimental data for the missile-shaped wooden ellipsoid.

The results of Figure 7 clearly demonstrate the effects of both angle of attack and velocity on the drag coefficient. It is evident that changes in the angle of attack have a more significant impact on the drag coefficient than changes in velocity. As the angle of attack increases, the drag coefficient experiences more substantial variations, highlighting its critical role in determining aerodynamic performance compared to velocity.

While interesting qualitative phenomena can be observed through the figures presented here, it is important to recognize the uncertainties of the experiment and how this can affect results. One major source of uncertainty was our small sample size. Since we were exporting data remotely, taking continuous samples would have resulted in file sizes too large to efficiently work with. For this reason, our data was collected through “snapshots” of 10 samples. 10 snapshots were taken per experiment, yielding 100 samples per experiment.

An additional major source of uncertainty in data collection was the angle of attack and wind speed. Both of these values were measured by Aerolab as well as by separate instruments. For wind speed, the external device measured a wind speed around 5-10 mph slower than recorded from Aerolab. For angle of attack, the angle measured using the digital protractor was about 0.7º off of the angle measured by Aerolab. Thus the wind speeds and angles that defined each experiment were not exact.

Discussion

The results demonstrate the effects of wind speed, and pitch angle on the drag forces and normal forces of all four objects with the results being in line with the hypothesis of the experiment. This experiment demonstrated that the wooden ellipsoid is the most aerodynamic shape tested, resulting in the lowest drag coefficient confirming our hypothesis. Additionally, it highlighted the strong correlation between wind speed, pitch angle, and the resultant drag and normal forces. These findings are consistent with the theoretical predictions and provide valuable insights into the aerodynamic behavior of objects under varying conditions.

The changes in wind speed and pitch significantly impact the drag force, as illustrated in Figures 2 through 7. These figures show that the relationship between drag force, wind speed, and pitch is not entirely linear, aligning with the quadratic nature of the drag force equation (Equation 2). The drag force is also influenced by the object's frontal area, which is evident in Figure 4, where objects with larger frontal areas exhibit higher drag forces. However, it’s important to note that the geometry of the frontal area plays a critical role in determining drag force beyond just its size. For instance, while a sphere may have a larger frontal area than an inverted sphere, the inverted sphere has a higher drag coefficient. This highlights how the shape and flow characteristics around the object contribute to drag; the geometry of the inverted sphere generates more turbulence and resistance, despite its smaller frontal area. Thus, both the size and the geometry of the frontal area are key factors in the drag force experienced by an object

The pitch angle significantly affected both the drag and normal forces. As the pitch angle increased, the drag force increased as well. This result aligns with theoretical expectations derived from the drag force equation, which considers the normal force component when summing vector forces. A similar trend was noted for the normal force: as the pitch angle increased, so did the normal force. This makes sense because, at a 0° pitch angle, the wind is perpendicular to the normal force component. However, as the pitch angle changes, both the wind and normal force develop components pointing in the same direction, leading to their addition or subtraction. Positive pitch angles resulted in an increase in normal force, while negative angles led to a decrease.

Despite a majority of the results conforming to predictions, it is important to mention the limitations of this analysis and sources of error. The primary source of error is the wind speed calculated by Aerolab. The Aerolab system relied on an input of temperature and humidity to perform the velocity calculation. Since these values are input manually, the precision of the measuring instrument is now a source of uncertainty. Additionally the experiment was performed over two separate laboratory sessions on different days with varied temperature and humidity conditions. While humidity and temperature measurements were taken on both days, it is unclear the effect this may have had on the wind velocity calculation performed internally by the Aerolab software. Additionally, when wind speed was measured using an external instrument, there was a deviation of ~10 mph or 4.5 m/s from the wind speed displayed in Aerolab. This brings into to question both the accuracy of the calculation and precision of the measurements taken to calculate wind speed, leading to uncertainty.

Conclusions and recommendations

The primary objective of this experiment was to compare the aerodynamic properties of different shaped objects by analyzing how wind speed and pitch angle affect drag force. Based on the data collected and the corresponding plots, it is evident that the wooden ellipsoid demonstrated the most aerodynamic efficiency, with the smallest drag coefficient and producing the least drag force. This result confirms that streamlined shapes, like the ellipsoid, are effective at reducing drag when moving through a fluid due to their ability to minimize resistance. As shown in Figure 5, the wooden ellipsoid consistently exhibited minimal drag across varying wind speeds and pitch angles, in contrast to the other tested objects, which experienced drag increases of up to 50% as speed and pitch angle increased. To improve the accuracy of this experiment and reduce errors, it is important to acknowledge that data collection presented challenges. The results varied significantly, and calculations were based on averaged data from multiple trials, which may not fully capture the true aerodynamic performance of each shape. The limitations inherent in measuring fluid motion likely contributed to these variations. Moving forward, the experiment could be refined by taking more precise and consistent measurements across a larger sample size. This would provide a more accurate depiction of the aerodynamic effects of each shape, leading to a deeper understanding of how geometry and fluid dynamics interact. Additionally, improving the calibration of measurement instruments and reducing environmental variables could enhance the reliability of the results.

References: [1]“Aerolab Educational Wind Tunnel (EWT) Owners Manual”, 2005

Statement of contribution:

Elijah Perez: Data Analysis, Figure, Theory, and Derivation, Lab Report.
Soham Saha: Experimental Design, Data Collection, Lab Report.
Alex Pham: Experimental Design, Data Collection, Lab Report**.**

Appendix

ρ = Density of fluid

A = Frontal area of object

V = Relative fluid velocity

C_D = Coefficient of drag

C_L = Coefficient of lift

r = Radius

L = Depth

$$A_{ellipsoid} \approx 2 \cdot \pi [\frac{(r \cdot L)^{1.6} + (r \cdot L)^{1.6} + (r^2)^{1.6}}{3}]^{\frac{1}{1.6}} \tag{3}$$

$$A_{Inverted} \approx 2 \cdot \pi r^2 + [\pi R^2 - \pi r^2] \tag{4}$$

$$A_{Sphere} \approx 2\pi r^2 \tag{5}$$

$$A_{plate} \approx \pi r^2 \tag{6}$$

Data unit conversions:

```
%% Gathering Cell data from sheets
Missle   = readtable("Missle.csv");
Sphear   = readtable("Sphear.csv");
Inverted = readtable("Inverted.csv");
Disk     = readtable("Disk.csv");
%% Convert to SI
% Missle
Missle(:,4)   = Missle(:,4)./2.237;              %MPH to m/s
Missle(:,5)   = Missle(:,5).*6895;               %Psi to Pa
for i = 1:600
Missle(i,6)   = (Missle(i,6)-32).*(5/9) + 273.15;    %F to K
end
Missle(:,8)   = Missle(:,8).*248.8;              %water In to pa
Missle(:,9)   = Missle(:,9).*248.8;              %water In to pa
Missle(:,10)  = Missle(:,10).*4.44822;             %LBF to N
Missle(:,11)  = Missle(:,11).*4.44822;             %LBF to N
Missle(:,12)  = Missle(:,12).*4.44822;             %LBF to N
% Sphear
Sphear(:,4)   = Sphear(:,4)./2.237;              %MPH to m/s
Sphear(:,5)   = Sphear(:,5).*6895;               %Psi to Pa
for i = 1:600
Sphear(i,6)   = (Sphear(i,6)-32).*(5/9) + 273.15;    %F to K
end
Sphear(:,8)   = Sphear(:,8).*248.8;              %water In to pa
Sphear(:,9)   = Sphear(:,9).*248.8;              %water In to pa
Sphear(:,10)  = Sphear(:,10).*4.44822;             %LBF to N
Sphear(:,11)  = Sphear(:,11).*4.44822;             %LBF to N
Sphear(:,12)  = Sphear(:,12).*4.44822;             %LBF to N
% Inverted
Inverted(:,4)   = Inverted(:,4)./2.237;          %MPH to m/s
Inverted(:,5)   = Inverted(:,5).*6895;           %Psi to Pa
for i = 1:600
Inverted(i,6)   = (Inverted(i,6)-32).*(5/9) + 273.15;  %F to K
end
Inverted(:,8)   = Inverted(:,8).*248.8;          %water In to pa
Inverted(:,9)   = Inverted(:,9).*248.8;          %water In to pa
Inverted(:,10)  = Inverted(:,10).*4.44822;         %LBF to N
Inverted(:,11)  = Inverted(:,11).*4.44822;         %LBF to N
Inverted(:,12)  = Inverted(:,12).*4.44822;         %LBF to N
```

Separation of data to respected experiment:

```
% MISSLE
MissleExp1 = table2array(Missle(1:100,4:end));       %Deg:0   ,V:50 mph
MissleExp2 = table2array(Missle(101:200,4:end));    %Deg:15  ,V:50 mph
MissleExp3 = table2array(Missle(201:300,4:end));    %Deg:30  ,V:50 mph
MissleExp4 = table2array(Missle(301:400,4:end));    %Deg:0   ,V:85 mph
MissleExp5 = table2array(Missle(401:500,4:end));    %Deg:15  ,V:85 mph
MissleExp6 = table2array(Missle(501:600,4:end));    %Deg:30  ,V:85 mph
% Sphear
SphearExp1 = table2array(Sphear(1:100,4:end));       %Deg:0   ,V:50 mph
SphearExp2 = table2array(Sphear(101:200,4:end));    %Deg:15  ,V:50 mph
SphearExp3 = table2array(Sphear(201:300,4:end));    %Deg:30  ,V:50 mph
SphearExp4 = table2array(Sphear(301:400,4:end));    %Deg:0   ,V:65 mph
SphearExp5 = table2array(Sphear(401:500,4:end));    %Deg:15  ,V:65 mph
SphearExp6 = table2array(Sphear(501:600,4:end));    %Deg:30  ,V:65 mph
% Inverted
InvertedExp1 = table2array(Inverted(1:100,4:end));   %Deg:0   ,V:50 mph
InvertedExp2 = table2array(Inverted(101:200,4:end)); %Deg:15  ,V:50 mph
InvertedExp3 = table2array(Inverted(201:300,4:end)); %Deg:30  ,V:50 mph
InvertedExp4 = table2array(Inverted(301:400,4:end)); %Deg:0   ,V:65 mph
InvertedExp5 = table2array(Inverted(401:500,4:end)); %Deg:15  ,V:65 mph
InvertedExp6 = table2array(Inverted(501:600,4:end)); %Deg:30  ,V:65 mph
% Plate
DiskExp1 = table2array(Disk(1:100,4:end));          %Deg:0   ,V:50 mph
DiskExp2 = table2array(Disk(101:200,4:end));        %Deg:15  ,V:50 mph
DiskExp3 = table2array(Disk(201:300,4:end));        %Deg:30  ,V:50 mph
DiskExp4 = table2array(Disk(301:400,4:end));        %Deg:0   ,V:65 mph
DiskExp5 = table2array(Disk(401:500,4:end));        %Deg:15  ,V:65 mph
DiskExp6 = table2array(Disk(501:600,4:end));
```

(Area)

```
%Area calcs
AreaMissle   = 0.00614608; % m^2
AreaSphear   = 0.06280000; % m^2
AreaInverted = 0.01809800; % m^2
AreaPlate    = 0.03305800; % m^2
```